Synthesis, Structure, and Characterization of $Ce_{1-x}A_xTiO_3$ ($0.0 \leq x \leq 0.8$; A = Sr, Ba)

Joseph E. Sunstrom, IV,† Susan M. Kauzlarich,*,† and Mark R. Antonio‡

Department of Chemistry, University of California, Davis, Davis, California 95616, and BP Research, 4440 Warrensville Center Rd., Cleveland, Ohio 44128-2837

Received July 21, 1992. Revised Manuscript Received November 19, 1992

The investigation of the solid solution $Ce_{1-x}A_xTiO_3$ (A = Sr, Ba) was undertaken with the aim to understand the magnetic and electronic properties as a function of alkaline earth doping. The solid solutions $Ce_{1-x}A_xTiO_3$ (A = Sr, Ba; $0.0 \leq x \leq 0.8$) have been prepared by arc melting stoichiometric amounts of $CeTiO_3$ and $ATiO_3$ under argon. Single-phase samples of $Ce_{1-x}Sr_xTiO_3$ can be made for the entire stoichiometry range. However, there is phase separation in samples of $Ce_{1-x}Ba_xTiO_3$ for high values of x. The polycrystalline samples have been characterized using microprobe, thermal gravimetric analysis, powder X-ray diffraction, Ce L-edge X-ray absorption fine structure, temperature- and field-dependent magnetization, and dc electrical resistivity. The $Ce_{1-x}Sr_xTiO_3$ samples crystallize in the orthorhombic space groups *Pbnm* ($x \leq 0.4$) and *Ibmm* ($0.4 < x \leq 0.8$). The $Ce_{1-x}Ba_xTiO_3$ samples crystallize in the orthorhombic space groups *Pbnm* ($x \leq 0.2$) and *Ibmm* ($0.2 < x \leq 0.6$). The $Ce_{0.2}Ba_{0.8}TiO_3$ sample is biphasic containing an orthorhombic phase (*Ibmm*) and a hexagonal $BaTiO_{3-x}$ phase. Ce XANES (X-ray absorption near-edge structure) data show that in all samples the Ce valence is 3+. The samples $Ce_{1-x}Sr_xTiO_3$ ($x = 0.0, 0.2$) exhibit a ferromagnetic component below 135 K due to coupling between Ce and Ti moments. The temperature dependent resistivity measurement on polycrystalline $CeTiO_3$ shows it to be a small gap (0.005 eV) semiconductor. The $Ce_{1-x}Sr_xTiO_3$ samples are metallic up to $x = 0.8$ while the $Ce_{1-x}Ba_xTiO_3$ samples are metallic for $x = 0.2, 0.4$.

Introduction

Since the discovery of high-temperature superconducting oxides, there has been a renewed interest in the study of structure–property relationships in metallic transition metal oxides. This group and others have studied the magnetic and electronic properties of $La_{1-x}A_xTiO_3$ (A = Sr, Ba) with an aim to prepare an n-type superconductor.[1,2] The metal–insulator boundary for a series of compounds, $Ln_{1-x}Ba_xTiO_3$ (Ln = La, Nd, Gd, Er, Y), has also been the subject of a recent study.[3] Although not superconducting, these oxides are metallic over a large value of x which is dependent upon the identity of the alkaline earth cation. These materials do not exhibit long-range magnetic ordering for the majority of compositions ($x \geq 0.05$ (Sr); $x > 0.00$ (Ba)). The investigation of the $Ce_{1-x}A_xTiO_3$ system is of interest since the rare earth ion (Ce^{III}) orders magnetically and is not associated with the conduction band. Although superconductivity was not observed in the $La_{1-x}A_xTiO_3$ system, the study of these solid solutions provides fundamental information that is important for understanding why superconductivity exists in some oxides and not others.[4]

The coexistence of long-range ferromagnetic order and superconductivity has been a long standing question in superconductivity physics.[5] The Chevrel phases which are molybdenum chalcogenides of the formula $A_xMo_6X_8$ (X = S, Se, Te; A = almost any metal ion) are one type of compounds that display ferromagnetic order and superconductivity.[6] With the discovery of high-T_c superconductivity in oxide materials, there is a large potential for discovering new ferromagnetic superconducting compounds. The study of the solid solution where one end member is ferromagnetic ($La_xSr_{1-x}MnO_3$) and the other is a high-T_c superconductor ($La_xSr_{1-x}CuO_3$) is an attempt to prepare a ferromagnetic, superconducting compound.[7] Many of the high-temperature superconductors are antiferromagnets, and currently none are known to exhibit long-range ferromagnetic behaviour.[8]

The structure and properties of $CeTiO_3$ have been studied in some detail.[9-14] This compound has two unpaired electrons: the Ti(III) $3d^1$ electron and the Ce-

† University of California.
‡ BP Research.

(1) (a) Sunstrom, J. E., IV; Kauzlarich, S. M.; Klavins, P. *Chem. Mater.* **1992**, *4*, 346. (b) Kauzlarich, S. M.; Sunstrom, J. E. IV; Klavins, P. *NIST Special Publication 804, Proceedings of the International Conference of the Chemistry of Electronic Ceramic Materials*; Davies, P. K., Roth, R. S., Eds.; 1991; p 217. (c) Sunstrom, J. E., IV; Kauzlarich, S. M. MRS Proceedings—Better Ceramics through Chemistry V; *Mat. Res. Soc. Symp. Proc.* **1992**, *271*, 107.

(2) (a) Maeno, Y.; Awaji, S.; Matsumoto, H.; Fujita, T. *Physica B* **1990**, *165, 166*, 1185. (b) Higuchi, M.; Aizawa, K.; Yamaya, K.; Kodaira, K. *J. Solid State Chem.* **1991**, *92*, 573. (c) Abbate, M.; de Groot, F. M. F.; Fuggle, J. C.; Fujimori, A.; Tokura, Y.; Fujishima, Y.; Strebel, O.; Domke, M.; Kaindl, G.; van Elp, J.; Thole, B. T.; Sawatzky, G. A.; Sacchi, M.; Tsuda, N. *Phys. Rev. B: Condens. Matter* **1991**, *44*, 5419. (d) Fujishima, Y.; Tokura, Y.; Arima, T.; Uchida, S. *Physica C* **1991**, *185*, 1001.

(3) Eylem, C.; Sàghi-Szabò, G.; Chen, B.-H.; Eichhorn, B.; Peng, J.-L.; Greene, R.; Salamanca-Riba, L.; Nahm, S. *Chem. Mater.* **1992**, *4*, 1038.

(4) (a) Torrance, J. B. *J. Solid State Chem.* **1992**, *96*, 8209. (b) Torrance, J. B.; Lacorre, P.; Asavaroengchai, C.; Metzger, R. M. *Physica C* **1991**, *182*, 351.

(5) Machida, K. *Appl. Phys. A* **1984**, *35*, 193.

(6) (a) Chevrel, R.; Sergent, M.; Prigent, J. *J. Solid State Chem.* **1971**, *3*, 515. (b) Shelton, R. N.; McCallum, R. W.; Adrian, H. *Phys. Lett.* **1976**, *56A*, 213. (c) Fischer, O. *Appl. Phys.* **1976**, *16*, 1.

(7) Haupt, L.; Schünemann, J.-W.; Bärner, K.; Sondermann, U.; Rager, B.; Abdelouhab, R. M.; Braunstein, R.; Dong, S. *Solid State Commun.* **1989**, *72*, 1093.

(8) For a review, see: Johnston, D. C. *J. Magn. Magn. Mater.* **1991**, *100*, 218.

0897-4756/93/2805-0182$04.00/0

Table I. Lattice Parameters for $Ce_{1-x}A_xTiO_3$ (A = Ba, Sr) Determined from Guinier X-ray Powder Diffraction

x	a	b	c	space group
		$Ce_{1-x}Sr_xTiO_3$		
0.0	5.604 (5)	5.589 (2)	7.870 (3)	*Pbnm*
0.2	5.556 (5)	5.532 (2)	7.870 (1)	*Pbnm*
0.4	5.544 (4)	5.519 (3)	7.842 (4)	*Pbnm*
0.6	5.552 (1)	5.522 (2)	7.821 (1)	*Ibmm*
0.8	5.540 (2)	5.521 (3)	7.810 (2)	*Ibmm*
		$Ce_{1-x}Ba_xTiO_3$		
0.0	5.604 (5)	5.589 (2)	7.870 (3)	*Pbnm*
0.2	5.587 (3)	5.583 (1)	7.902 (6)	*Pbnm*
0.4	5.610 (6)	5.582 (2)	7.901 (1)	*Ibmm*
0.6	5.594 (4)	5.583 (3)	7.918 (3)	*Ibmm*
0.8	5.641 (5)	5.572 (3)	7.924 (4)	*Ibmm*[a]

[a] Two-phase mixture.

(III) $4f^1$ electron. The magnetic structure of $CeTiO_3$ consists of a noncollinear ferromagnetically ordered Ce(III) sublattice and a canted antiferromagnetic (G-type) Ti(III) sublattice.[14] The ferromagnetic ordering of the Ce(III) is induced by the Ti(III) moments.[14] There is no significant Ce–Ce interaction as evidenced by the analogous compound $CeScO_3$.[15] $CeTiO_3$ and $LaTiO_3$ are the only metallic rare earth titanates, each having room-temperature resistivities on the order of 10^{-2}–10^{-3} Ω cm.[11] The conductivity of this compound is the result of delocalization of the 3d electron through a conduction band of π symmetry. The unpaired electrons in this compound exist in two different environments. The $4f^1$ electron associated with cerium is capable of exhibiting localized, ferromagnetic behaviour while the titanium $3d^1$ electron can be delocalized causing metallic and possibly superconducting properties. Observation of ferromagnetism and superconductivity may be possible in this system due to these two different electron environments.

The determination of the valence of cerium in oxides is a matter of intensive effort in catalysis[16–18] and corrosion[19–21] sciences. It is now common practice to use cerium L-edge X-ray absorption fine structure (XAFS) to provide direct information about cerium valence in solutions[22] and solids.[23] Cerium L_3-edge XAFS has been successfully applied to many systems, such as CeO_x (for $1.5 < x < 2.0$) and alloys. The oxidation state of cerium in $Ce_{1-x}A_xTiO_3$ (A = Sr, Ba; $0.0 \leq x \leq 0.8$) has been determined by cerium L-edge XANES, X-ray absorption near edge structure. With this information about cerium in $Ce_{1-x}A_xTiO_3$, the effects of the alkaline earth cations on the magnetic and electronic properties can be determined.

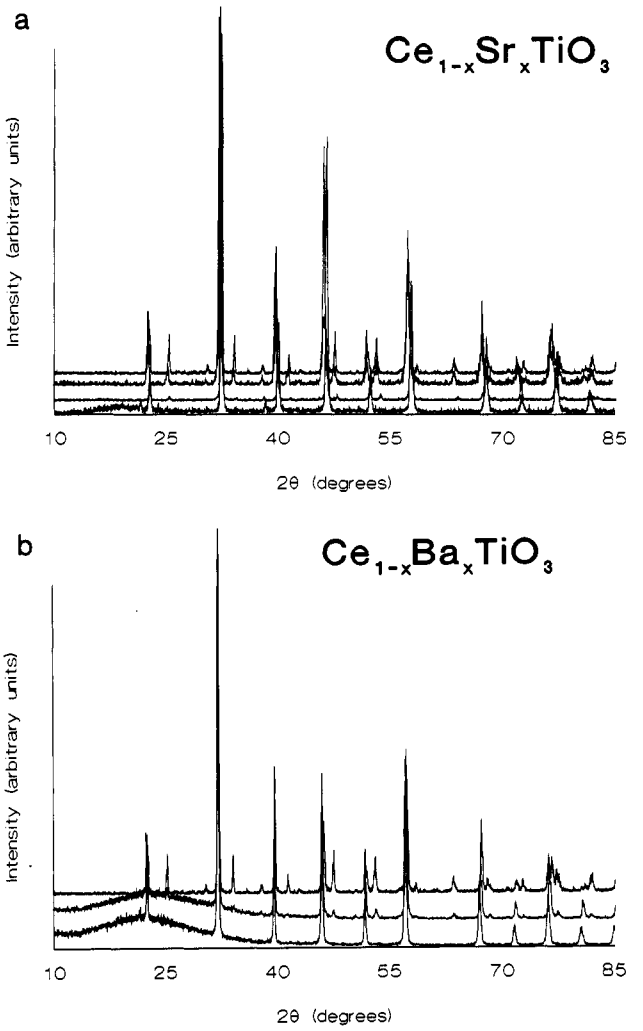

Figure 1. (a) Powder X-ray diffractometer traces of $Ce_{1-x}Sr_xTiO_3$ for (from top to bottom) (1) $x = 0.0$, (2) $x = 0.2$, (3) $x = 0.4$, (4) $x = 0.6$. (b) Powder X-ray diffractometer traces of $Ce_{1-x}Ba_xTiO_3$ for (from top to bottom) (1) $x = 0.0$, (2) $x = 0.2$, (3) $x = 0.4$.

Experimental Section

Materials. TiO_2 (99.999%), $SrCO_3$ (99.999%), and $BaCO_3$ (99.99%) were purchased from Johnson Matthey. They were dried for 24 h at 120 °C prior to use. Ti metal (20 mesh granules, 99.99%) was used as purchased from Johnson Matthey. CeO_2 was heat treated at 1300 °C for 24 h prior to use.

Synthesis. $ATiO_3$ (A = Sr, Ba) was prepared by standard ceramic methods. Three grinding and firing cycles were usually needed to obtain pure $SrTiO_3$ (*Pm3m*, $a = 3.905$ Å)[24] and $BaTiO_3$ (*P4mm*, $a = 3.994$ Å, $c = 4.037$ Å).[25]

Stoichiometric amounts of Ti metal and TiO_2 were arc melted under argon to make TiO. The oxygen content of the TiO was determined by oxidation to be 1.00 ± 0.05 using thermal gravimetric analysis. CeO_2 and TiO and then arc melted under argon in a 1:1 stoichiometric ratio to form $CeTiO_3$ (*Pbnm*, $a = 5.570$ Å, $b = 5.584$ Å, $c = 7.865$ Å).[14] All $CeTiO_3$ samples used

(9) (a) Brous, J.; Fankuchen, I.; Banks, E. *Acta Crystallogr.* **1953**, *16*, 67. (b) Holzapfel, H.; Sieler, J. *Z. Anorg. Allg. Chem.* **1966**, *343*, 174. (c) Sieler, J.; Hennig, H. *J. Prakt. Chem.* **1966**, *34*, 168.
(10) (a) Bazuev, G. V.; Shveikin, G. P. *Zh. Neorg. Khim.* **1977**, *22*, 1239. (b) Bazuev, G. V.; Shveikin, G. P. *Izv. Akad. Nauk SSR, Neorg. Mater.* **1978**, *14*, 267. (c) Bazuev, G. V.; Shveikin, G. P. *Fiz. Tverd. Tela.* **1975**, *11*, 3453.
(11) MacLean, D. A.; Greedan, J. E. *Inorg. Chem.* **1981**, *20*, 1025.
(12) Greedan, J. E. *The Rare Earths in Modern Science and Technology*; McCarthy, G. J., Silber, H. E., Rhyne, J. J., Eds.; Plenum: New York, 1982; Vol. 2.
(13) Greedan, J. E. *J. Less Common Met.* **1985**, *111*, 335.
(14) Goral, J. P.; Greedan, J. E. *J. Magn. Magn. Mater.* **1983**, *37*, 315.
(15) Turner, C. W.; Greedan, J. E. *J. Solid State Chem.* **1980**, *34*, 207.
(16) Antonio, M. R.; Brazdil, J. F.; Glaeser, L. C.; Mehicic, M.; Teller, R. G. *J. Phys. Chem.* **1988**, *92*, 2338.
(17) Le Normand, F.; Hilaire, L.; Kili, K.; Krill, G.; Maire, G. *J. Phys. Chem.* **1988**, *92*, 2561.
(18) Dauscher, A.; Hilaire, L.; Le Normand, F.; Muller, W.; Maire, G.; Vasquez, A. *Surf. Interface Anal.* **1990**, *16*, 341.
(19) Davenport, A. J.; Isaacs, H. S.; Kendig, M. W. *Corros. Sci.* **1991**, *32*, 653.
(20) Davenport, A. J.; Isaacs, H. S.; Kendig, M. W. *J. Electrochem. Soc.* **1989**, *136*, 1837.
(21) Fransen, T.; Gellings, P. J.; Fuggle, J. C.; van der Laan, G.; Esteva, J. M.; Karnatak, R. C. *Appl. Surf. Sci.* **1985**, *20*, 257.
(22) (a) Sham, T. K. *J. Chem. Phys.* **1983**, *79*, 1116. (b) Prieto, C.; Lagarde, P.; Dexpert, H.; Briois, V.; Villain, F.; Verdaguer, M. *J. Phys. Chem. Solids* **1992**, *53*, 233.

for synthesis in the solid solutions have a O:Ti ratio of 3.00 ± 0.02.

Solid solutions of $Ce_{1-x}A_xTiO_3$ (A = Sr, Ba; $0.0 \leq x \leq 0.80$) were prepared by arc melting stoichiometric quantities of $CeTiO_3$ and $ATiO_3$ (A = Sr, Ba) under an argon atmosphere.

Structure. X-ray powder diffraction data were obtained using an Enraf-Nonius Guinier camera equipped with a Johannson monochromator. Typical procedures have been described previously.[1a] Calculated powder patterns for $CeTiO_3$ (*Pbnm*), $SrTiO_3$ (*Pm3m*), and $BaTiO_3$ (*P4mm*) were made using the computer program POWDER.[26] A standard least-squares fitting program was used to calculate lattice parameters for the series (Table I). The lattice parameters for $CeTiO_3$, $SrTiO_3$, and $BaTiO_3$ are in agreement with their respective literature values.

A second set of X-ray diffraction data was obtained on a Siemens D-500 with Cu Kα radiation. The diffractometer traces shown in Figure 1, were examined to check peak splitting, peak shapes, and intensity values.

Oxygen Content Analysis. Oxygen stoichiometry was determined using a Du Pont 2100 thermal analyzer. The microbalance on the thermal gravimetric unit was calibrated before every experiment. Approximately 100 mg of sample was placed in a platinum boat hung from the microbalance. The samples were heated from 25 to 1000 °C at 5 °C/min in 50 cm^3/min flowing O_2. The furnace was allowed to isotrack at 900 °C for 6 h during the run to ensure complete oxidation.

Elemental Analysis. Cation (Ce, Sr, Ba, Ti) stoichiometries were determined using a Cameca SX50 electron microprobe on alumina polished samples. Ce and Ti stoichiometry for the $CeTiO_3$ sample were determined using CeO_2 and $SrTiO_3$ as standards. The $CeTiO_3$ sample was then used as a standard to determine Ce concentration in the solid solutions. The other standards used for the solid solutions were $SrTiO_3$ (Sr and Ti) and $BaSO_4$ (Ba).

XAFS Measurements. Cerium L-edge XAFS data were obtained on beam line X-18B at the NSLS (National Synchrotron Light Source), Brookhaven National Laboratory, operating at 2.5 GeV with ca. 110–220 mA of stored current. A double-crystal Si(220) monochromator was used for the Ce L_1-, L_2-, and L_3-edge scans at 6548, 6164, and 5723 eV, respectively. The X-ray beam size on the samples was 1×17 mm^2. All cerium L-edge X-ray absorption data were collected at ambient temperature with the electron-yield technique in order to avoid thickness effects and to provide accurate edge resonance intensities and peak positions.[27,28] Each specimen (in the form of irregularly shaped black "beads") was stuck on metalized polyester film tape (3M No. 850) and then taped to the back plane of a flow-type electron-yield detector (The EXAFS Co.). Helium was used as an ionization detector for the electron-yield signal, I_e. The incident X-ray intensity, I_0, was measured with a sealed ion chamber proportional counter filled with nitrogen to provide an absorbance of ca. 0.1 at 6000 eV. To minimize the harmonic content of I_0, the orientation of the crystals was adjusted to pass ca. 50% of the maximum incident photon intensity at every wavelength throughout the scan. The relative energy calibration was maintained to ±0.1 eV throughout the course of data collection. For reference purposes, the Cr K-edge XANES and first differential XANES for a chromium film (500 Å) on glass were used for absolute energy calibration. The energy of the inflection point in the first differential Cr XANES data was observed at 5995.2 ± 0.1 eV (cf. supplementary material). All data were obtained with integration times of 2 s/point for the Ce L_2- and L_3-edge XANES and 3 s/point for the Ce L_1-edge XANES. Each spectrum was obtained at uniform energy steps of 2 eV/point for the pre- and postedge regions and 0.5 eV/point for the XANES regions. As described elsewhere,[15,29] the primary X-ray absorption data, I_e/I_0, were normalized by use of least-squares approximations (two-term linear functions) to the pre- and postedge signals. The Ce L_1-, L_2-, and L_3-edge data were independently normalized to provide edge jumps of unity. Interferences from the barium L_2- and L_1-edge resonances (5624 and 5989 eV, respectively) for $Ce_{1-x}Ba_xTiO_3$ (x = 0.6 and 0.8) prevented an accurate normalization of the Ce L_3- and L_2-edge XANES. Although the Ba L_2- and L_1-edge peaks were observed in the Ce XANES for $Ce_{1-x}Ba_xTiO_3$ (x = 0.4 and 0.2), their low intensities did not adversely affect the normalization. To obtain the Ce L_3- and L_2-edge resonance widths and positions, the data were fit with the program (EDGFIT) and procedure of Lytle et al.[30] The XANES was adequately modeled with the sum of Lorentz and arctangent functions convolved with a 2.5-eV Gaussian line-broadening function.[16]

Magnetic Measurements. A Quantum Design SQUID magnetometer was used to make magnetic measurements. Samples were powdered and placed into evacuated quartz tubes for measurement. The samples were measured using an applied field of 1 T from 10 to 300 K. Magnetization vs field data (hysteresis loops) were measured for the $CeTiO_3$, $Ce_{0.8}Sr_{0.2}TiO_3$, and $Ce_{0.8}Ba_{0.2}TiO_3$ samples from −5 to 5 T at 10 K. In addition, all samples were screened for the Meissner effect at 5 K.

Electrical Resistivity. Temperature-dependent dc resistivity was measured using a standard four-probe technique. Sample preparation has been described previously.[1a] Samples were measured from 15 to 300 K. Reversal of current bias was used to minimize thermal voltages.

Results and Discussion

Synthesis. The study of a conducting $Ti^{III/IV}$–O octahedral network and its interaction with the magnetic Ce sublattice requires control of the Ce(III) and Ti(III,-IV) valences. $Ce_{1-x}A_{1-x}TiO_3$ (A = Sr, Ba) can be readily synthesized by formation of solid solutions of $CeTiO_3$ and $ATiO_3$. Because there are structural similarities between the end members of the solid solution, the enthalpy of mixing is low and most of the compositional range can be made. To obtain the starting material, $CeTiO_3$, with Ce and Ti in their reduced trivalent state, it is necessary to reduce CeO_2 with TiO under argon. It is also possible to obtain Ce(III) by the reduction of CeO_2 to Ce_2O_3 and use

(23) (a) Bianconi, A.; Marcelli, A.; Dexpert, H.; Karnatak, R.; Kotani, A.; Jo, T.; Petiau, J. *Phys. Rev. B: Condensed Matter* **1987**, *35*, 806. (b) Karnatak, R. C.; Esteva, J. M.; Dexpert, H.; Gasgnier, M.; Caro, P. E.; Albert, L. *Phys. Rev. B: Condensed Matter* **1987**, *36*, 1745. (c) Dexpert, H.; Karnatak, R. C.; Esteva, J. M.; Connerade, J. P.; Gasgnier, M.; Caro, P. E.; Albert, L. *Phys. Rev. B: Condensed Matter* **1987**, *36*, 1750. (d) Karnatak, R. C.; Esteva, J. M.; Dexpert, H.; Gasgnier, M.; Caro, P. E.; Albert, L. *J. Magn. Magn. Mater.* **1987**, *63*, *64*, 518. (e) Karnatak, R. C.; Gasgnier, M.; Dexpert, H.; Esteva, J. M.; Caro, P. E.; Albert, L. *J. Less-Common Met.* **1985**, *110*, 377. (f) Lengeler, B.; Materlik, G.; Muller, J. E. *Phys. Rev. B: Condensed Matter* **1983**, *28*, 2276. (g) Beaurepaire, E.; Krill, G.; Kappler, J. P.; Rohler, J. *Solid State Commun.* **1984**, *49*, 65. (h) Malterre, D.; Krill, G.; Durand, J.; Marchal, G.; Ravet, M. F. *Phys. Rev. B: Condens. Matter* **1986**, *34*, 2176. (i) Godart, C.; Gupta, L. C.; Ravet-Krill, M. F. *J. Less-Common Met.* **1983**, *94*, 187. (j) Malterre, D. *Phys. Rev. B: Condens. Matter* **1991**, *43*, 1391. (k) Wohlleben, D.; Rohler, J. *J. Appl. Phys.* **1984**, *55*, 1904. (l) Neifeld, R. A.; Croft, M.; Mihalisin, T.; Segre, C. U.; Madigan, M.; Torikachvili, M. S.; Maple, M. B.; DeLong, L. E. *Phys. Rev. B: Condens. Matter* **1985**, *32*, 6928. (m) Raaen, S.; denBoer, M. L.; Murgai, V.; Parks, R. D. *Phys. Rev. B: Condens. Matter* **1983**, *27*, 5139. (n) Parks, R. D.; Raaen, S.; denBoer, M. L.; Murgai, V.; Mihalisin, T. *Phys. Rev. B: Condens. Matter* **1983**, *28*, 3556. (o) Mihalisin, T.; Harrus, A.; Raaen, S.; Parks, R. D. *J. Appl. Phys.* **1984**, *55*, 1966. (p) Scoboria, P.; Harrus, A.; Andraka, B.; Mihalisin, T.; Raaen, S.; Parks, R. D. *J. Appl. Phys.* **1984**, *55*, 1969. (q) Buffat, B.; Chevalier, B.; Tuilier, M. H.; Lloret, B.; Etourneau, J. *Solid State Commun.* **1986**, *59*, 17.

(24) Megaw, H. D. *Proc. Phys. Soc. (London)* **1946**, *A189*, 261.

(25) Harada, J.; Pedersen, T.; Barnea, Z. *Acta Crystallogr.* **1970**, *A26*, 336.

(26) Clark, C. M., Smith, D. K., Johnson, G. J. *A. Fortran IV Program for Calculating X-ray Powder Diffraction Patterns—Version V*; Department of Geosciences: The Pennsylvania State University, University Part, PA, 1973.

(27) Lytle, F. W. In *Applications of Synchotron Radiation*; Winick, H., Xian, D.; Ye, M. H., Huang, T., Eds.; Gordon and Breach: New York, 1988; Vol. 4, p 135.

(28) Elam, W. T.; Kirkland, J. P.; Neiser, R. A.; Wolf, P. D. *Phys. Rev. B: Condens. Matter* **1988**, *38*, 26.

(29) Antonio, M. R.; Song, I.; Yamada, H. *J. Solid State Chem.* **1991**, *93*, 183.

(30) Lytle, F. W.; Greegor, R. B.; Panson, A. J. *Phys. Rev. B: Condens. Matter* **1988**, *37*, 1550.

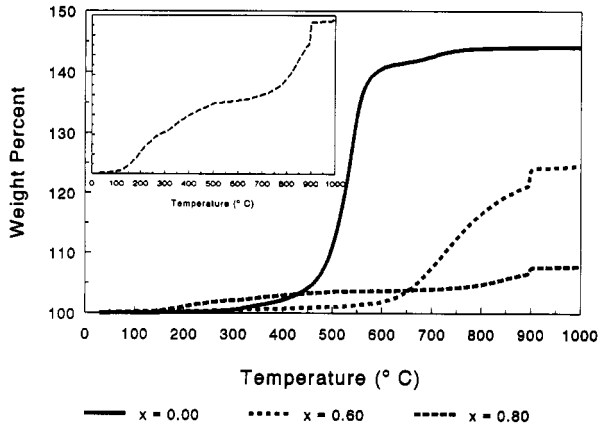

Figure 2. Thermal gravimetric analysis data of $Ce_{1-x}Ba_xTiO_3$ heated under flowing O_2 (50cc/min) (from top to bottom) (1) x = 0.0, (2) x = 0.6, (3) x = 0.8. Inset: expanded view of $Ce_{0.2}Ba_{0.8}TiO_3$ which shows oxygen weight gain beginning at 100 °C.

Table II. Cation Stoichiometries Determined from Microprobe Analysis and Oxygen Stoichiometries Determined from Thermal Gravimetric Analysis

$Ce_{1.02(4)}TiO_{2.99}$	
$Ce_{0.87(2)}Ba_{0.20(1)}TiO_{2.99}$	$Ce_{0.78(5)}Sr_{0.23(6)}TiO_{3.00}$
$Ce_{0.71(3)}Ba_{0.42(4)}TiO_{3.00}$	$Ce_{0.57(5)}Sr_{0.43(4)}TiO_{3.01}$
$Ce_{0.59(7)}Ba_{0.58(6)}TiO_{3.00}$	$Ce_{0.40(2)}Sr_{0.56(2)}TiO_{3.01}$
$Ce_{0.41(9)}Ba_{0.87(10)}TiO_{2.91}$	$Ce_{0.18(3)}Sr_{0.80(2)}TiO_{2.96}$

ceramic methods to produce $CeTiO_3$, but this requires high temperature (1450 °C) and a reducing atmosphere (H_2 or NH_3).[31] The absence of Ce(IV) is important in order to obtain $Ce_{1-x}A_xTiO_3$ with Ti in the B site of the perovskite structure. CeO_2 is similar in reactivity to TiO_2, and it is possible to form $BaCeO_3$[32] and/or $CeTi_2O_6$.[33] Previous studies of the CeO_2–BaO–TiO_2 phase diagram[34] indicate that $BaCeO_3$ is quite soluble in $BaTiO_3$. In the compound $BaCeO_3$, Ce(IV) is octahedrally coordinated by oxygen. However, based on radius ratios, Ce(III) is too big to have octahedral coordination with oxygen and $BaCeO_3$ should not form in the absence of Ce(IV). Diluting the $CeTiO_3$ with $ATiO_3$ permits the study of a partially oxidized Ti–O framework without oxidation of the Ce from +III to +IV. No evidence for $BaCe_xTi_{1-x}O_3$ or $CeTi_2O_6$ is seen in samples prepared in this manner.

Oxygen Content. The oxygen content determined by TGA for each composition is summarized in Table II. The TGA traces for three samples ($CeTiO_3$, $Ce_{0.4}Ba_{0.6}TiO_3$, $Ce_{0.2}Ba_{0.8}TiO_3$) heated under flowing O_2 are shown in Figure 2.

It has been proposed that the oxidation of $CeTiO_3$ occurs in two stages: formation of a poorly crystalline $CeO_{2-\delta}$·$TiO_{2-\delta}$ intermediate phase, and second-stage oxidation of $CeO_{2-\delta}$·$TiO_{2-\delta}$ occurring with crystallization of CeO_2.[35] These two steps account for the large weight gain at 500 °C and the smaller weight gain at 700 °C, respectively. Our TGA data for $CeTiO_3$ is in good agreement with the previous result.[35]

The oxygen content for $Ce_{1-x}A_xTiO_3$ is 3.00 ± 0.01 for $x \leq 0.6$. The x = 0.8 samples are oxygen deficient for both the Sr- and Ba-doped $CeTiO_3$ compounds. We have previously proposed that because oxygen is in the coordination sphere of the A cation in the ABO_3 compounds, it will be easier to create oxygen vacancies around a +2 alkaline earth than a +3 rare earth based on electrostatic attraction. Another possible explanation for the oxygen deficiency at high molar concentrations of $ATiO_3$ is attributed to the arc melting technique. As the conducting $CeTiO_3$ is diluted with the insulating $ATiO_3$, much longer arc melting times and higher temperatures are required for complete reaction. The oxygen content in these samples can be reduced by long arc melting times. Evidence for oxygen deficiency in the alkaline-earth-rich samples can be seen in the TGA traces where the oxygen uptake temperature increases to about 600 °C with x until x = 0.6. This oxygen weight gain is due to oxidation of Ce and Ti to their tetravalent oxidation states. For $Ce_{0.2}Ba_{0.8}TiO_3$, the sample begins to uptake oxygen at 100 °C and then again at 700 °C (Figure 2). This indicates that there are oxygen deficiencies in the structure which appear to be associated with the 2+ cation so that the A-rich materials are better represented by a two-phase mixture, $ATiO_{3-x}$–$CeTiO_3$. The initial weight gain at 150 °C is due to oxygen vacancies being filled and the second weight gain at 700 °C is due to oxidation of the Ce and Ti from the trivalent state to the tetravalent state. Two phases, one which crystallizes in the hexagonal $BaTiO_{3-x}$ structure[36] and the other which crystallizes in the orthorhombic *Ibmm* perovskite structure can also be detected in the X-ray powder diffraction.

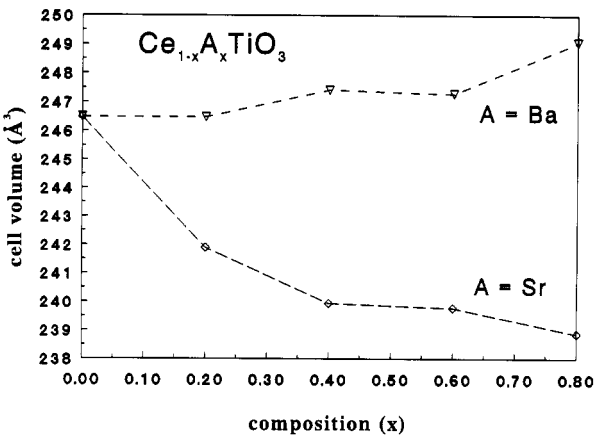

Figure 3. Plot of cell volume vs composition of $Ce_{1-x}A_xTiO_3$ (top A = Ba, bottom A = Sr) for compositions $x \leq 0.8$.

Elemental Analysis. The structure and properties of $RETiO_3$ (RE = rare earth) have been shown to vary with cation stoichiometry.[37] The microprobe results and standard deviations for the compounds studied are shown in Table II. The compounds will be referred to by the as-prepared stoichiometries in the remainder of the text. The $CeTiO_3$ sample, which was used to make all the compounds, is on stoichiometry within the standard deviation. The standard deviations for the $Ce_{1-x}Sr_xTiO_3$ and $Ce_{1-x}Ba_xTiO_3$ samples are based on a sampling of 8–10 points on the sample, and give some indication of homogeneity in the samples. The standard deviations of the $Ce_{1-x}Sr_xTiO_3$ indicate the samples are fairly homogenous. The Ce_{1-x}-

(31) Leonov, A. I.; Piryutko, M. M.; Keler, E. K. *Izv. Akad. Nauk SSSR Ser. Khim.* **1966**, *5*, 787. Eng. Transl.: *Bull. Acad. Sci. (Div. of Chem. Sci.)* **1966**, *5*, 756.
(32) Keler, E. K.; Godina, N. A.; Kalinina, A. M. *Zh. Neorg. Khim.* **1956**, *1*, 2556.
(33) Roth, R. S.; Negas, T.; Parker, H. S.; Minor, D. B.; Jones, C. *Mater. Res. Bull.* **1977**, *12*, 1173.
(34) Guha, J. P.; Kolar, D. *J. Am. Ceram. Soc.* **1973**, *56*, 5.
(35) Bazuev, G. V.; Makarova, O. V.; Zhilyaev, V. A.; Shveikin, G. P. *Russ. J. Inorg. Chem.* **1976**, *21*, 1447.
(36) Burbank, R. D.; Evans, H. T. *Acta Crystallogr.* **1948**, *1*, 330.
(37) (a) Bazuev, G. V.; Makarova, O. V.; Shveikin, G. P. *Izv. Akad. Nauk SSSR, Neorg. Mater.* **1983**, *19*, 108. (b) Bazuev, G. V.; Makarova, O. V.; Shveikin, G. P. *Zh. Neorg. Khim.* **1978**, *23*, 1451. (c) Kestigian, M.; Ward, R. *J. Am. Chem. Soc.* **1955**, *77*, 6199.

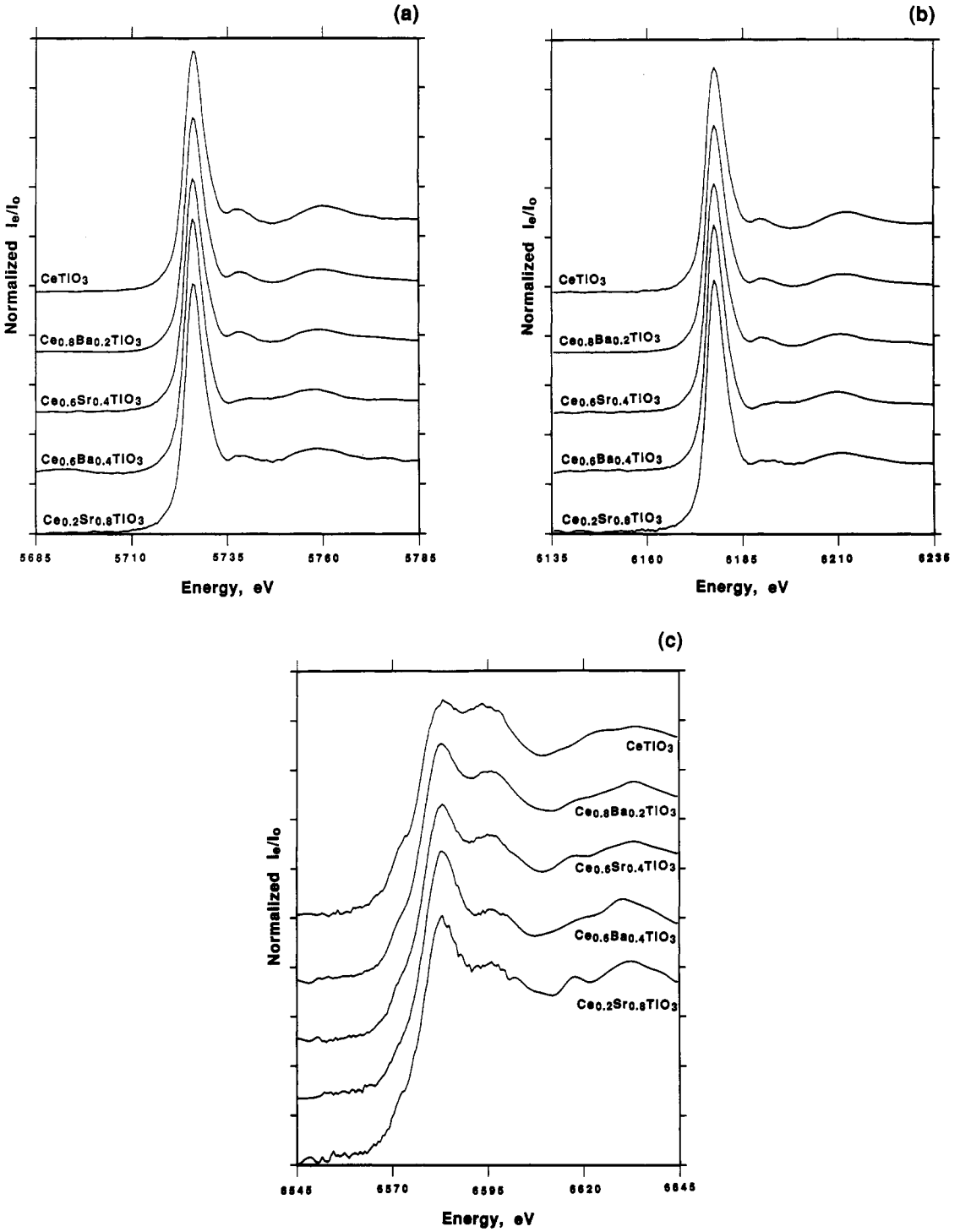

Figure 4. Cerium L-edge XANES for $CeTiO_3$, $Ce_{0.8}Ba_{0.2}TiO_3$, $Ce_{0.6}Sr_{0.4}TiO_3$ (*Pbnm* structure type) and $Ce_{0.6}Ba_{0.4}TiO_3$, $Ce_{0.2}Sr_{0.8}TiO_3$ (*Ibmm* structure type): (a) Ce L_3-edge; (b) Ce L_2-edge; (c) Ce L_1-edge.

Ba_xTiO_3 samples are homogeneous for the $x = 0.2$, 0.4 samples. The $x = 0.6$ shows heterogeneity and the $x = 0.8$ is biphasic. Inefficient mixing of $CeTiO_3$ and $BaTiO_3$ may be attributed to the large size difference between the Ce^{3+} and Ba^{2+} cations. Oxygen deficient $BaTiO_3$ crystallizes in a hexagonal structure type which consists of TiO_6 octahedra which are partially edge shared. This hexagonal structure may not be amenable to mixing with the $LnTiO_3$ structure type ($GdFeO_3$).

The microprobe data for the $Ce_{1-x}Ba_xTiO_3$ (ABO_3) samples show excess cations in the A site. For example, the $Ce_{0.4}Ba_{0.6}TiO_3$ samples contains almost a 20% excess of Ce/Ba cations on the A site giving rise to the stoichiometry of $Ce_{0.59(7)}Ba_{0.58(6)}TiO_{3.00}$. However, an additional phase cannot be detected by X-ray powder diffraction and it is not possible to achieve an A site stoichiometry of greater than 1 in the perovskite (ABO_3) structure type. The excess of Ce/Ba cations on this site gets larger with increasing $BaTiO_3$ concentration and is probably due to the choice of standards used for analysis ($BaSO_4$). The standard $SrTiO_3$ was used for the microprobe data in the case of the $Ce_{1-x}Sr_xTiO_3$ samples whose stoichiometries are in agreement with the expected stoichiometry.

Structure. The lattice parameters for $Ce_{1-x}A_xTiO_3$ (A = Sr, Ba; $0.0 \le x \le 0.8$) are summarized in Table I. $CeTiO_3$ has been indexed in the orthorhombic space group *Pbnm*.

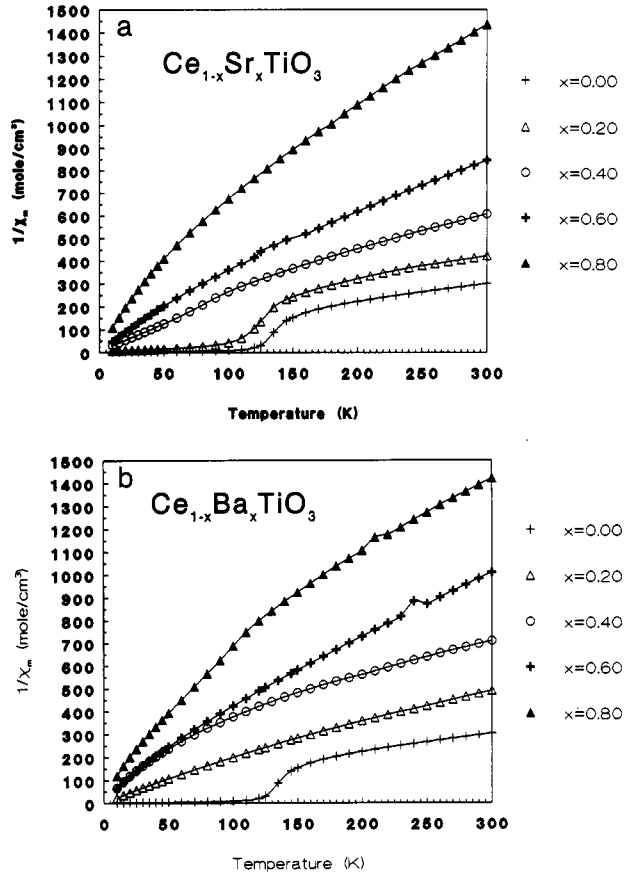

Figure 5. (a) Temperature-dependent magnetic susceptibilities (10–300 K range) of $Ce_{1-x}Sr_xTiO_3$ plotted as $1/\chi_m$ vs temperature for (from top) (1) $x = 0.8$, (2) $x = 0.6$, (3) $x = 0.4$, (4) $x = 0.2$, (5) $x = 0.0$. (b) Temperature-dependent magnetic susceptibilities (10–300 K range) of $Ce_{1-x}Ba_xTiO_3$ plotted as $1/\chi_m$ vs temperature for (from top) (1) $x = 0.8$, (2) $x = 0.6$, (3) $x = 0.4$, (4) $x = 0.2$, (5) $x = 0.0$.

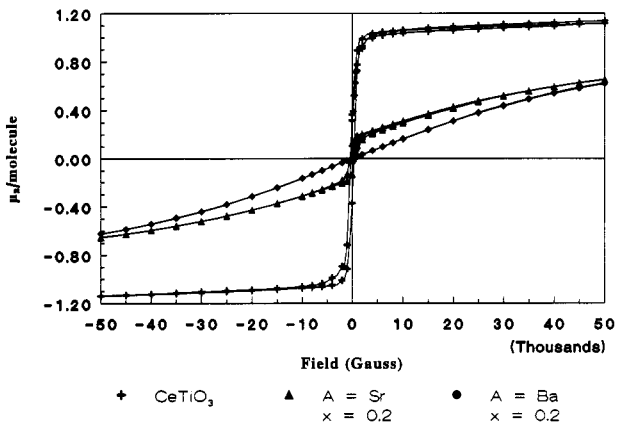

Figure 6. Magnetic field hysteresis loops for $CeTiO_3$, $Ce_{0.8}Sr_{0.2}TiO_3$, and $Ce_{0.8}Ba_{0.2}TiO_3$ taken at 10 K.

For $CeTiO_3$, $c/a < \sqrt{2}$ which means it is designated O′-orthorhombic because of a superimposed Jahn–Teller distortion. The Jahn–Teller distortion is not present in the $x = 0.2$ sample of $Ce_{1-x}Sr_xTiO_3$ or $Ce_{1-x}Ba_xTiO_3$. The Goldschmidt tolerance factor[38]

$$t = R_A + R_O/\sqrt{2}(R_B + R_O)$$

is less than 0.9 for compounds in the *Pbnm* space group

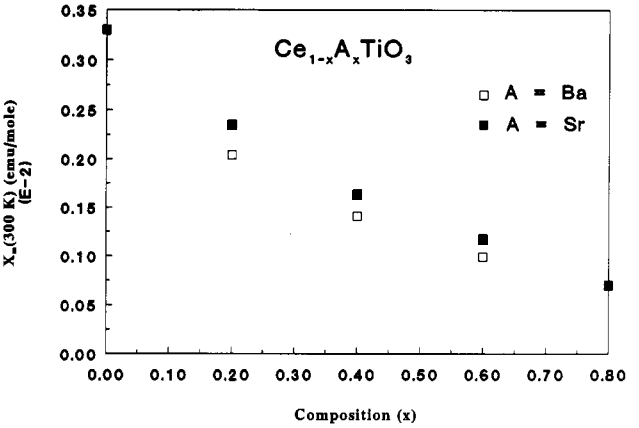

Figure 7. Room-temperature susceptibilities (χ_m(300 K)) vs composition for compositions $x \leq 0.8$.

(R_A, R_B, and R_O are the radii for the A cation, B cation, and oxygen; respectively, in ABO_3 compounds). Using Shannon–Prewitt radii (Ce^{3+}, 1.285 Å; Ba^{2+}, 1.50 Å; Sr^{2+}, 1.40 Å; Ti^{3+}, 0.81 Å; Ti^{4+}, 0.745 Å; O^{2-}, 1.21 Å),[39] the Goldschmidt factor predicts the $Ce_{1-x}Sr_xTiO_3$ and $Ce_{1-x}Ba_xTiO_3$ compounds will retain the *Pbnm* structure type until $x = 0.39$ and $x = 0.26$, respectively. Parts a and b of Figure 1 show the X-ray powder diffraction patterns for $0 \leq x \leq 0.6$ (Sr) and $0 \leq x \leq 0.4$ (Ba), respectively. The weak reflections attributed to the *Pbnm* structure type are clearly absent for the $x = 0.6$ (Sr) and $x = 0.4$ (Ba) samples in agreement with the prediction based on the Goldschmidt tolerance factor. The $x = 0.4$ sample is still the *Pbnm* structure type for the $Ce_{1-x}Sr_xTiO_3$ compound but not for the $Ce_{1-x}Ba_xTiO_3$ compound. The remaining $Ce_{1-x}Sr_xTiO_3$ samples ($x = 0.6$, 0.8) and $Ce_{1-x}Ba_xTiO_3$ ($x = 0.4$, 0.6, 0.8) could be indexed in the orthorhombic space group Ibmm which is a subgroup of the *Pm3m* (cubic) and supergroup of the *Pbnm* (orthorhombic) space groups.[40]

Figure 3 shows the cell volume vs composition for both the $Ce_{1-x}Sr_xTiO_3$ and $Ce_{1-x}Ba_xTiO_3$ series. The cell volume decreases for the $Ce_{1-x}Sr_xTiO_3$ series with increasing x but increases slightly for the $Ce_{1-x}Ba_xTiO_3$ series. The average oxidation state and average radius of the Ti^{3+}/Ti^{4+} cation should be the same for any given composition x for both $Ce_{1-x}Sr_xTiO_3$ and $Ce_{1-x}Ba_xTiO_3$. The volume expansion in the $Ce_{1-x}Ba_xTiO_3$ series can therefore be attributed to the larger average size of the Ce^{3+}/Ba^{2+} cation. In the $Ce_{1-x}Sr_xTiO_3$ series, the size of the Ce^{3+}/Sr^{2+} cation becomes less important than the contraction of the Ti–O framework due to the smaller average radius of the Ti^{3+}/Ti^{4+} cation. This leads to a decrease in cell volume with increasing x in $Ce_{1-x}Sr_xTiO_3$. The same general trend was noted for the $La_{1-x}A_xTiO_3$ (A = Sr, Ba) series.[1a,c]

Biphasic regions at low x have been proposed based on HREM studies of $Ln_{1-x}Ba_xTiO_3$ (Ln = La, Nd).[3] X-ray diffraction studies were not able to confirm this, and there is no evidence of a biphasic region at low x in these samples.

Ce XANES Data. The normalized XANES for the cerium L_3-, L_2-, and L_1-edges of $CeTiO_3$, $Ce_{1-x}Ba_xTiO_3$ ($x = 0.2$, and 0.4) and $Ce_{1-x}Sr_xTiO_3$ ($x = 0.4$ and 0.8) are displayed in Figure 4. As shown, intense, narrow resonances are found at the L_3- and L_2-edges (5726.2 ± 0.1 and 6177.8 ± 0.1 eV, respectively) of the Ce XANES for every phase of the $Ce_{1-x}A_xTiO_3$ (A = Ba, Sr and $0.0 < x < 0.8$)

(38) Goodenough, J. B.; Longo, J. M. In *Landolt-Börnstein Tabellen*, New Series III/4a; Springer-Verlag: Berlin, 1970.

(39) Shannon, R. D.; Prewitt, C. T. *Acta Crystallogr.* **1969**, *B25*, 925.
(40) Bärnighausen, H. *Acta Crystallogr. A* **1975**, *S3*, 31.

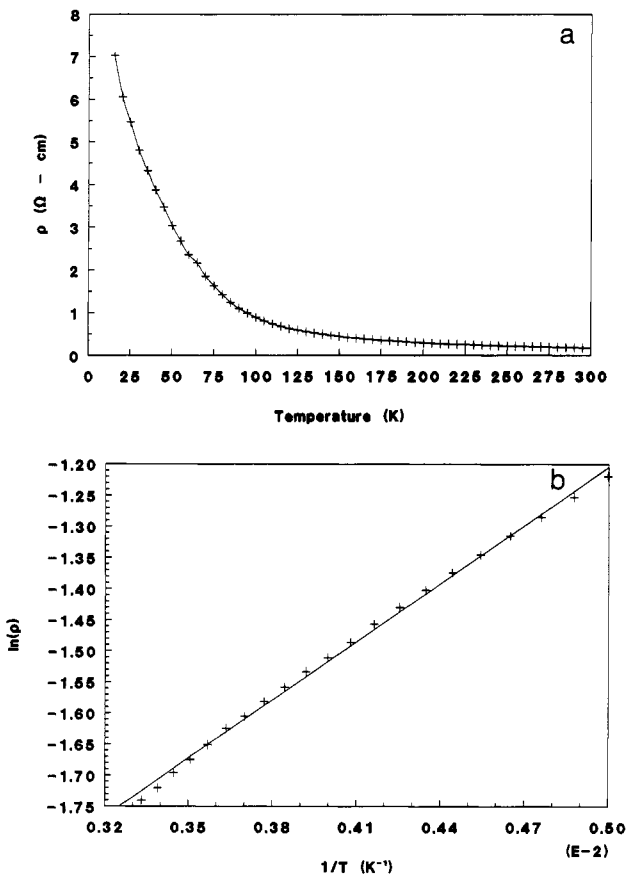

Figure 8. (a) Resistivity (ρ) vs temperature (10–300 K) for $CeTiO_3$. (b) Plot of ln ρ vs $1/T$ for the high-temperature range (200–300 K).

solid solution. These edge resonance profiles are typical of trivalent cerium, Ce^{III}.[15-18,21,22a,c,f,h,41] All compounds with formally trivalent cerium ions (e.g., $Ce_xBi_{2-x}[MoO_4]_3$ for $0.025 < x < 1.5$,[15] $Ce_2(CO_3)_3{\cdot}5H_2O$,[15] $Ce(NO_3)_3{\cdot}nH_2O$,[16] Ce_2O_3,[16] $Ce(OH)_3$,[16,17] $CeCl_3{\cdot}7H_2O$,[18] $CePO_4$,[41] etc.) exhibit similar single resonances. In comparison, the Ce L_3- and L_2-edge XANES of compounds with formally quadrivalent cerium ions (e.g., CeO_2,[15-18,22a,c,e,40a,42] $[NH_4]_2Ce(NO_3)_6$,[15] $Ce(SO_4)_2{\cdot}4H_2O$,[22a] etc.) exhibit two strong edge resonances. Hence, the use of Ce L_3- and L_2-edge XANES provides an excellent fingerprint of Ce valence. The L_3- and L_2-edge peaks correspond to electronic (dipole) transitions from the Ce $2p_{3/2}$ and $2p_{1/2}$ initial states, respectively, to the empty Ce 5d orbital manifold, i.e., $5d_{3/2}$ and $5d_{5/2}$ for the L_3-edge and $5d_{3/2}$ for the L_2-edge. The descriptive ground state configuration of Ce(III) is $[Xe]4f^15d^0$, and the excited-state configuration is $[Xe]4f^15d^1$ with a "hole" in the 2p manifold, i.e., $2p^5$. The L_2- and L_3-edge XANES for each phase in $Ce_{1-x}A_xTiO_3$ (A = Ba, Sr and $0.0 < x < 0.8$) are almost identical, cf. Figure 4a,b. This indicates that the excited state is an admixture of overlapping $5d_{3/2}$ and $5d_{5/2}$ states, and the splitting of the final 5d states due to spin–orbit coupling is negligible in comparison to the 5d bandwidth.[43,44] A rough estimate of the 5d bandwidth is provided by the fwhm line widths of the L_3-edge and L_2-edge resonances, 4.0–4.9 and 3.6–4.2 eV, respectively. The range in line widths (and intensities) is attributed to differences in band structure of $Ce_{1-x}A_xTiO_3$ as a function of A content, x. Although the L_3- and L_2-edge resonances do not change with either x or A in $Ce_{1-x}A_xTiO_3$, the two higher energy peaks at ca. 5738 and 5760 eV (L_3-edge, Figure 4a) and 6190 and 6211 eV (L_2-edge, Figure 4b), due to photoelectron backscattering (i.e., EXAFS), reveal subtle changes in shape through the *Pbnm–Ibmm* structural transition. These peaks in the spectra for $CeTiO_3$, $Ce_{0.8}Ba_{0.2}TiO_3$, and $Ce_{0.6}Sr_{0.4}TiO_3$ with the *Pbnm* structure type (top three spectra in Figure 4a,b) are sharper and more pronounced than those for $Ce_{0.6}Ba_{0.4}TiO_3$ and $Ce_{0.2}Sr_{0.8}TiO_3$ with the *Ibmm* structure type (bottom two spectra in Figure 4a,b). A similar effect is observed in the L_1-edge XANES data, Figure 4c, as a difference in the relative intensities of the two edge peaks at ca. 6583 and 6595 eV. For the phases with the *Ibmm* structure (e.g., $Ce_{0.6}Ba_{0.4}TiO_3$ and $Ce_{0.2}Sr_{0.8}TiO_3$, bottom two spectra in Figure 4c), the low-energy peak is ca. 20% more intense than the high-energy peak, whereas for the phases with the *Pbnm* structure (e.g., $Ce_{0.8}Ba_{0.2}TiO_3$ and $Ce_{0.6}Sr_{0.4}TiO_3$), the low energy peak is ca. 10% more intense than the high energy peak. For $CeTiO_3$ (*Pbnm*, top spectrum, Figure 4c), the two peaks are of nearly equal intensity. These Ce L-edge data illustrate the general result of the so-called "join" between L_1- and $L_{2,3}$-edge XANES and EXAFS, wherein the inverted L_1-edge EXAFS matches the L_2- and L_3-edge EXAFS,[41,45] (cf. supplementary material). The absence of well-resolved peaks on or before the Ce L_1 absorption edge centered at ca. 6578 eV for $Ce_{1-x}A_xTiO_3$ (A = Ba, Sr and $0.0 < x < 0.8$) indicates that the Ce^{III} ions are in a site of high symmetry. Cerium L_1-edge XANES involves an electronic (dipole) transition from the Ce 2s initial state to the empty 6p orbital manifold. Electronic transitions from the 2s to 5d manifold have also been identified in L_1-edge XANES as preedge peaks.[41,46] The cross section for 2s → 5d transitions depends upon, in large part, the site symmetry of the absorbing atom. That is, preedge peaks are very weak for atoms in a site with inversion symmetry and increase in intensity as the site is distorted or the inversion symmetry is removed. For a tetrahedral coordination environment, the 2s → 5d transition is intense and well-resolved, whereas for an octahedral coordination environment, it is weak and unresolved. The Ce L_1-edge data of Figure 4c reveal a slight bulge on the edge near 6572. This is consistent with the slight distortion of the Ce(III)–O_8 polyhedra in $CeTiO_3$[14] and $Ce_{1-x}A_xTiO_3$. The presence of Ce^{3+} and Sr^{2+} for all x in $Ce_{1-x}Sr_xTiO_3$ is analogous to that of La^{3+} and Sr^{2+} in $La_{1-x}Sr_xTiO_3$ for $0.0 < x < 1.0$. The oxidation states of lanthanum and strontium in $La_{1-x}Sr_xTiO_3$ are constant with increasing Sr content, x: high-resolution titanium 2p X-ray absorption spectra reveal that the formal valence of titanium increases with x in $La_{1-x}Sr_xTiO_3$ from Ti^{III} ($x = 0$) to Ti^{IV} ($x = 1$).[2c] Similarly, the oxidation states of cerium (Ce^{III}) and strontium (Sr^{2+}) and barium (Ba^{2+}) in $Ce_{1-x}A_xTiO_3$ are constant as a function of A (Sr, Ba) content for $0.0 < x < 0.8$. Titanium 2p X-ray

(41) (a) Bauchspiess, K. R.; Boksch, W.; Holland-Moritz, E.; Launois, H.; Pott, R.; Wohlleben, D. In *Valence Fluctuations in Solids*; Falicov, L. M., Hanke, W., Maple, M. B., Eds.; North-Holland: New York, 1981; p 417. (b) Ravot, D.; Godart, C.; Achard, J. C.; Lagarde, P. *Ibid.*; p 423.
(42) Lytle, F. W.; van der Laan, G.; Greegor, R. B.; Larson, E. M.; Violet, C. E. *Phys. Rev. B: Condens. Matter* **1990**, *41*, 8955.
(43) Mannsour, A. N.; Cook, J. W.; Sayers, D. E. *J. Phys. Chem.* **1984**, *88*, 2330.
(44) Sham, T. K. *J. Am. Chem. Soc.* **1983**, *105*, 2269.
(45) (a) Lytle, F. W.; Greegor, R. B. *Appl. Phys. Lett.* **1990**, *56*, 192. (b) Chaboy, J.; Garcia, J.; Marcelli, A. *Solid State Commun.* **1992**, *82*, 939.
(46) Horsley, J. A.; Wachs, I. E.; Brown, J. M.; Via, G. H.; Hardcastle, F. D. *J. Phys. Chem.* **1987**, *91*, 4014.

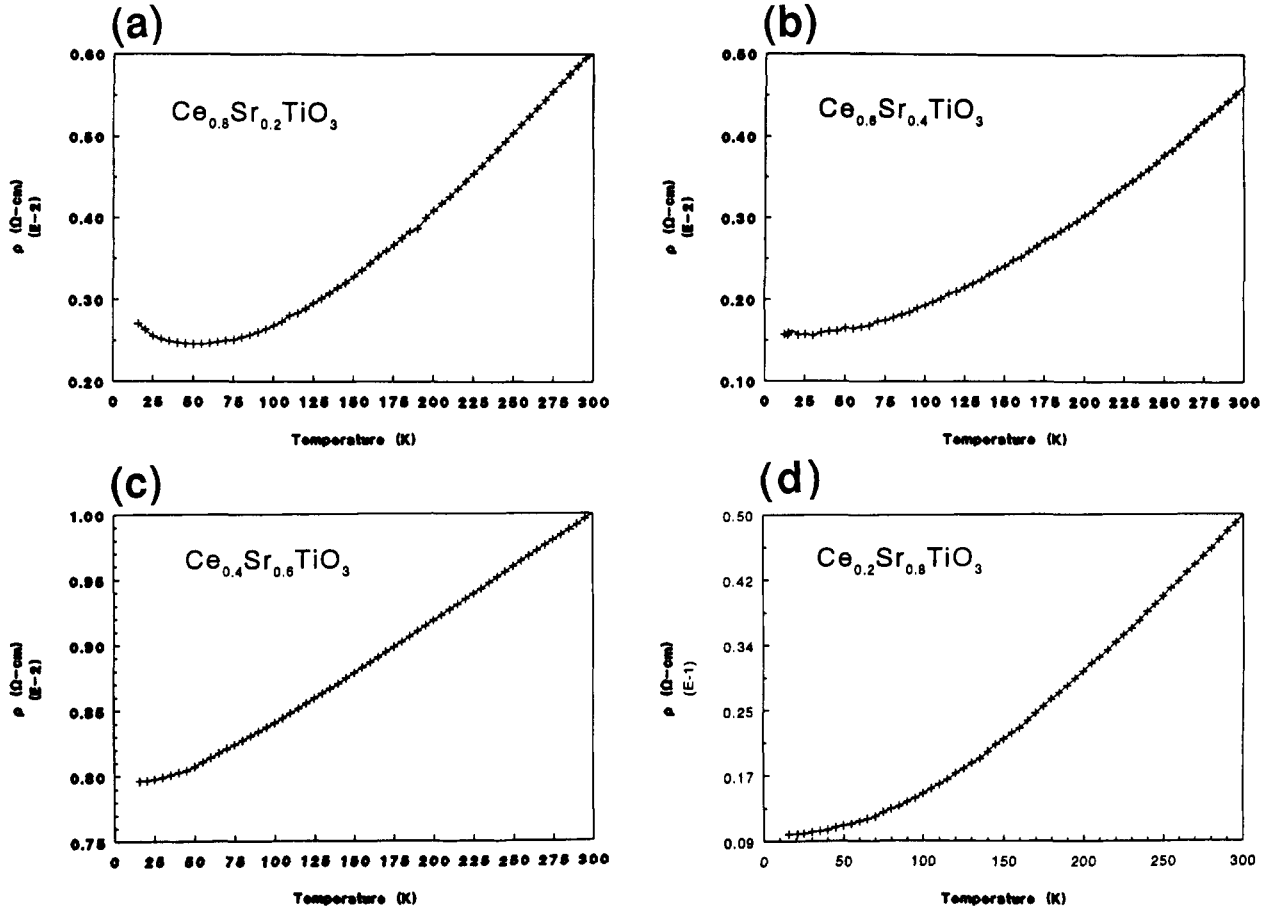

Figure 9. Plots of resistivity (ρ) vs temperature for (a) $Ce_{0.8}Sr_{0.2}TiO_3$, (b) $Ce_{0.6}Sr_{0.4}TiO_3$, (c) $Ce_{0.4}Sr_{0.6}TiO_3$, and (d) $Ce_{0.2}Sr_{0.8}TiO_3$.

absorption data are not available for $Ce_{1-x}A_xTiO_3$ for comparison with those data for $La_{1-x}Sr_xTiO_3$.

Magnetic Properties. Parts a and b of Figure 5 show the $1/\chi_m$ vs temperature data for all compositions of $Ce_{1-x}Sr_xTiO_3$ and $Ce_{1-x}Ba_xTiO_3$, respectively. Figure 6 shows the hysteresis loops of $Ce_{0.8}Sr_{0.2}TiO_3$ and $Ce_{0.8}Ba_{0.2}TiO_3$ along with the hysteresis loop of $CeTiO_3$. The polycrystalline $CeTiO_3$ sample has a ferromagnetic component due to Ce–Ti coupling with a Curie temperature of 125 K and a saturation moment of 0.97 (1) μ_B: both values are slightly higher than previously reported.[11] As with $LaTiO_3$,[47,48] the magnetic and electronic properties of $CeTiO_3$ strongly depend on the oxygen stoichiometry. Our data are on polycrystalline samples with the oxygen stoichiometry of 2.99, whereas Greedan's single-crystal sample is slightly oxidized with an oxygen stoichiometry of 3.013.[11] In the $Ce_{1-x}Sr_xTiO_3$ series, the $x = 0.2$ compound still shows ferromagnetic ordering at a lower T_c of 100 K. The hysteresis loop for the $Ce_{0.8}Sr_{0.2}TiO_3$ sample shows that the sample does not saturate up to 5 T. The hysteresis loop for the $Ce_{0.8}Ba_{0.2}TiO_3$ sample shows a slight dependence on field indicating that there is a small ferromagnetic component to the magnetism (see Figure 6). However, compared with $Ce_{0.8}Sr_{0.2}TiO_3$, $Ce_{0.8}Ba_{0.2}TiO_3$ does not exhibit magnetic order. Since the Ti^{III}/Ti^{IV} (4:1) ratio is the same for both the $Ce_{0.8}Sr_{0.2}TiO_3$ and $Ce_{0.8}Ba_{0.2}TiO_3$ samples, this indicates that the destruction of magnetic order depends on either the identity or size of the alkaline earth cation. In the case of $La_{1-x}A_xTiO_3$, the destruction of magnetic order occurs when the *Pbnm* structure changes from O′ to O orthorhombic structure.[1a,c] The absence/presence of magnetic ordering in $Ce_{1-x}A_xTiO_3$ (A = Sr, Ba) does not coincide with the loss of Jahn–Teller distortion. Both $Ce_{0.8}Sr_{0.2}TiO_3$ and $Ce_{0.8}Ba_{0.2}TiO_3$ are predicted to be the O-orthorhombic structure based on lattice parameter ratios (c_0/a_0) less than $\sqrt{2}$ and magnetic ordering is observed for the $Ce_{0.8}Sr_{0.2}TiO_3$ sample. Barium is larger than strontium, giving rise to longer Ti–O and Ce–O distances. Ba is also more electropositive than Sr and may give rise to better Ti(3d)–O(2p) π overlap. Either effect could lead to destruction of magnetic order for the Ba sample.

Parts a and b of Figure 5 show that T_{Curie} is lowered (125 K) for $Ce_{0.8}Sr_{0.2}TiO_3$ and that the remaining compositions for $Ce_{1-x}A_xTiO_3$ are paramagnets. The paramagnetism of the higher compositions is from a combination of Ti(III) $3d^1$ and Ce(III) $4f^1$ moments. It is difficult to resolve the contributions of both Ce(III) and Ti(III) to the magnetism as was noted for $CeTiO_3$.[11] The data can be fit to a simple Curie–Weiss law:

$$\chi_M = C/(T - \theta)$$

which neglects the χ_{TIP} term (TIP = temperature-independent paramagnetism). The fits to the simple Curie–Weiss show a decrease in the Curie constant (C) and effective moment (μ_{eff}) with increasing $ATiO_3$ (A = Sr, Ba) concentration. The Weiss constant (θ) for $CeTiO_3$ is −50.7 K and decreases with increasing alkaline earth concentration. This is consistent with the dilution of both the Ti^{III} and Ce^{III} magnetic cations. However, these

(47) Crandles, D. A.; Timusk, T.; Greedan, J. E. *Phys. Rev. B* **1991**, *44*, 13250.
(48) Lichtenberg, F.; Widmer, D.; Bednorz, J. G.; Williams, T.; Reller, A. *Z. Phys. Rev. B: Condens. Matter* **1991**, *82*, 211.

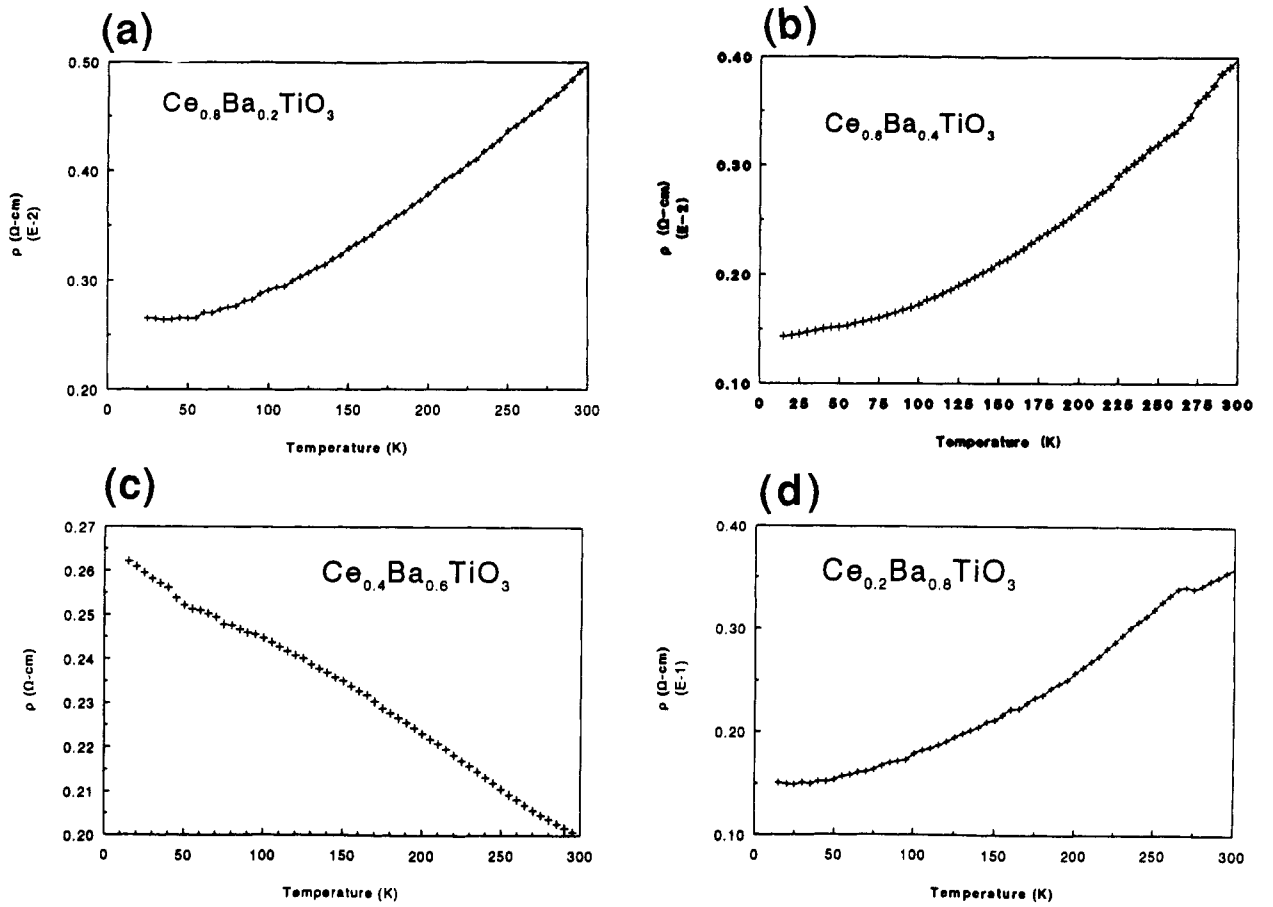

Figure 10. Plots of resistivity (ρ) vs temperature for (a) $Ce_{0.8}Ba_{0.2}TiO_3$, (b) $Ce_{0.6}Ba_{0.4}TiO_3$, (c) $Ce_{0.4}Ba_{0.6}TiO_3$, and (d) $Ce_{0.2}Ba_{0.8}TiO_3$.

materials are metallic and have been shown to have a large χ_{TIP} contribution to the magnetism.[1,11] If the temperature independent term is included in the Curie–Weiss fits for metallic compositions, a variety of C, θ, and χ_{TIP} values are obtained without any apparent trends. Significant curvature is present even in the high-temperature (160–300 K) data (see Figure 5). Since crystal-field effects can contribute and the contributions due to Ce and Ti cannot be quantified, no further attempt to fit the magnetic data was pursued.

Figure 7 shows the room-temperature molar susceptibilities plotted as a function of composition. The room temperature susceptibilities decrease in a smooth fashion. In the $La_{1-x}A_xTiO_3$ (A = Sr, Ba) series, the high-temperature susceptibilities (180–300 K) exhibit temperature independent paramagnetism from the delocalized Ti^{III} $3d^1$ electrons. There are discontinuities in the $La_{1-x}A_xTiO_3$ (A = Sr, Ba) compound χ_m(300 K) values as a function of temperature which we have attributed to changes in the DOS (density of states) that are a result of structural changes in the series.[1] In the $Ce_{1-x}A_xTiO_3$ (A = Sr, Ba) compounds, the χ_m(300 K) values are a combination of a the localized $4f^1$ electron (large effect) and a temperature independent term from the Ti $3d^1$ electron (small effect). The smooth decrease in the room temperature susceptibilities as a function of increasing alkaline earth metal doping is a consequence of the dilution of the localized Ce^{III} $4f^1$ moment. χ(300 K) is slightly smaller for Ba-doped samples vs Sr-doped samples and is most likely due to differences in stoichiometry rather than identity of the cation.

Electrical Properties. Figure 8a shows resistivity (ρ) vs temperature data for polycrystalline $CeTiO_3$. The data indicate the sample is semiconducting from 10 to 300 K. Figure 8b is a plot of ln ρ vs temperature (200–300 K) for the $CeTiO_3$ sample. A bandgap of 0.005 eV is calculated by fitting these data to a semiconductor model. Our result differs from resistivity results previously published on single-crystal $CeTiO_3$ which indicated that $CeTiO_3$ is metallic down to 60 K and then becomes semiconducting.[11] We have seen reproducible results on a number of samples whose composition is well-known and close to $CeTiO_{3.00}$. The room-temperature resistivity of polycrystalline $CeTiO_3$ is 0.17 Ω cm which is two orders of magnitude higher than the single-crystal study.[11] Although the magnitude of the polycrystalline $CeTiO_3$ resistivity also includes some unknown contribution from grain boundary resistance, the conductivity is clearly an activation type and not metallic. Two recent studies on $LaTiO_{3\pm x}$ indicate that slight changes in oxygen stoichiometry can greatly affect the electrical properties.[46,47] This appears to also be the case for $CeTiO_3$. The polycrystalline samples prepared in our study are slightly reduced (chemical formula $Ce_{1.02(4)}TiO_{2.99}$) and remained semiconducting over the entire temperature range studied. The previous result which showed the metal–semiconducting transition at 60 K was done on a slightly oxidized sample (chemical formula $CeTiO_{3.013}$).[11] An electronic property phase diagram was proposed by Lichtenberg et al. for $LaTiO_x$.[47] This phase diagram shows that stoichiometric $LaTiO_3$ is semiconducting over the entire temperature range, whereas slightly oxidized samples show a metal–semiconducting transition. The $CeTiO_3$ resistivity data collected in this study and the previous study[11] indicate that a similar phase diagram may be appropriate for $CeTiO_x$.

Figure 9 shows the resistivity vs temperature plots for the $Ce_{1-x}Sr_xTiO_3$ ($x = 0.2, 0.4, 0.6, 0.8$) samples. The $Ce_{0.8}Sr_{0.2}TiO_3$ sample shows a metallic temperature dependence down to 50 K then becomes semiconducting. The metal–semiconducting transition temperature in $Ce_{0.8}Sr_{0.2}TiO_3$ is lower than its T_{Curie} of 125 K. For $x = 0.4, 0.6, 0.8$, the $Ce_{1-x}Sr_xTiO_3$ samples have a metallic temperature dependence.

Figure 10 shows the resistivity vs temperature (10–300 K) plots for the four compositions of $Ce_{1-x}Ba_xTiO_3$. The $x = 0.2, 0.4$ samples have a metallic temperature dependence. The $x = 0.6$ sample shows a semiconducting temperature dependence. Heterogeneity in the $x = 0.6$ sample may be the cause of the semiconducting behavior. Regions which are more $BaTiO_3$ rich should have higher resistivity than $CeTiO_3$-rich areas. The $x = 0.8$ sample shows a metallic temperature dependence. Again, heterogeneity will play a role in the $x = 0.8$ sample. The $x = 0.8$ sample is oxygen deficient, which will make the $BaTiO_3$ rich domains more amenable to conduction.

Summary

Compounds with the composition $Ce_{1-x}Sr_xTiO_3$ can be made through the entire stoichiometry range. $Ce_{1-x}Ba_xTiO_3$ has phase separation with high concentrations of $BaTiO_3$ ($x \geq 0.6$) probably due to the widely different radii of Ba^{2+} and Ce^{3+} or structural imcompatibility between hexagonal $BaTiO_{3-x}$ and $CeTiO_3$ ($GdFeO_3$ structure). The compositions were found not to superconduct down to 5 K. These materials fit well into the phenomenological phase diagram proposed by Goodenough.[49] Prediction of magnetic and electrical properties is based on a quantity b, the transfer integral, which increases as the Ti–O–Ti angle gets closer to 180°. With increasing $ATiO_3$ (A = Sr, Ba) concentration, the transfer integral becomes larger and metallic properties predominate in the compounds. By use of cerium L-edge XANES, the oxidation state of cerium was found to be trivalent, Ce^{III}, for all phases in the $Ce_{1-x}A_xTiO_3$ (A = Ba, Sr and $0.0 \leq x \leq 0.8$) solid solution.

Acknowledgment. We thank R. N. Shelton for use of the diffractometer, TGA, and SQUID magnetometer, P. Klavins for technical assistance, and P. Schiffman for the microprobe data. We thank A. S. Bommannavar (X-18B) and M. S. Engbretson (Argonne National Laboratory) for assistance with the XAFS measurements at the NSLS, which is supported by the U.S. Department of Energy, Division of Materials Sciences and Division of Chemical Sciences. We also thank B. Eichhorn for useful discussion and a preprint of ref 3. This work was supported by National Science Foundation Solid State Chemistry Grant DMR-8913831.

Supplementary Material Available: Figures of chromium XANES and first differential XANES and the inverted L_1-edge XAFS and the L_3-edge XAFS of $CeTiO_3$ (4 pages). Ordering information is given on any current masthead page.

(49) Goodenough, J. B. *Prog. Solid State Chem.* 1971, 5, 145.